Asian Journal of Chemistry; Vol. 30, No. 9 (2018), 2116-2128

ASIAN JOURNAL OF CHEMISTRY

https://doi.org/10.14233/ajchem.2018.21482

Single Crystal XRD and Quantum Chemical Studies on Non-Proton Transfer Co-Crystals of 2-Amino-5-nitropyridine with Phenylthioacetic Acid and Barbituric Acid

V. VELMURUGAN[1], S. KUMARESAN[1,*], B. RAVINDRAN DURAI NAYAGAM[2], N. BHUVANESH[3], S. ATHIMOOLAM[4] and P. PALANISAMY[5]

[1]Department of Chemistry, Manonmaniam Sundaranar University, Abishekapatti, Tirunelveli-627 012, India
[2]Department of Chemistry, Pope's College, Sawyerpuram-628 251, India
[3]Department of Chemistry, Texas A & M University, College Station, Texas-77842, U.S.A.
[4]Department of Physics, University College of Engineering, Anna University, Nagercoil-629004, India
[5]Department of Chemistry, Pioneer Kumaraswamy College, Nagercoil-629 003, India

*Corresponding author: E-mail: skumarmsu@yahoo.com

Received: 26 May 2018; *Accepted*: 2 July 2018; *Published online*: 31 July 2018; AJC-19030

New co-crystals of 2-amino-5-nitropyridine with phenylthioacetic acid or barbituric acid have been grown by gradual evaporation approach under room temperature. The molecular structures of the present compounds were resolved by single crystal X-ray diffraction. The vibration spectral measurement was carried out using FT-IR spectroscopy. The X-ray studies show that the crystal packing is control by N–H···O and O–H···N for 2-amino-5-nitropyridine: phenylthioacetic acid (2A5NPPTAA) and N–H···O and N–H···N for 2-amino-5-nitropyridine: barbituric acid (2A5NPBBA), intermolecular hydrogen bonds leading to hydrogen bonded co-crystal. In 2A5NPPTAA, the 2-amino 5-nitropyridine (2A5NP) is linked with carboxyl group in phenylthioacetic acid (PTAA) through N–H···O intermolecular hydrogen bond to form ring $R_2^2(8)$ motifs. The N–H···O and O–H···N intermolecular hydrogen bonds are leading to a ring $R_4^4(8)$ motif. These ring motifs lead to the hydrophilic layers at z = 0 and 1 which are intermediate between the hydrophobic layer at 1/2. In the 2A5NPBBA, the N–H···O and N–H···N intermolecular hydrogen bonds form a heterosynthon of two $R_2^2(8)$ motifs. This ring motif is connected with nitro group in 2-amino-5-nitropyridine by N–H···O hydrogen bond to form a rare bifurcated ring $R_3^4(8)$ motif. These two ring motifs are further linked in barbituric (BBA) acid *via* N–H···O hydrogen bond to form $R_3^3(12)$ motifs. This molecular aggregations lead parallel to the 202 and $\bar{2}0\bar{2}$ crystallographic smooth making strong intensity peaks for these plain on X-ray diffraction. Computative optimizations of the molecules were done by density functional theory (DFT) using the B3LYP function and Hartree-Fock (HF) level with 6-311++G(d,p) basis set. The enhance molecular division and computed vibration spectrum are approximate experiment results which display express accepting.

Keywords: 2-Amino-5-nitropyridine, Phenylthioacetic acid, Barbituric acid, Co-crystal.

INTRODUCTION

Molecular co-crystals have obtained importance due to their ability towards physico-chemical properties [1]. Development of physical property of co-crystals like solubility, dissolution rate, melting point, colour, *etc*. require proper manipulative of co-formers [2]. Uses of co-crystals include pharmaceutical materials [3], electronic- and visible materials *etc*. [4,5]. Aminopyridines are a substantiate class of bio-active compounds [6]. The repetition of the hydrogen-bonded motifs leads to supramolecular architectures playing a considerable role in crystal engineering [7,8]. Koshima *et al.* [9] described the syntheses and NLO properties of the co-crystals of 2-amino-5-nitropyridine and benzenesulfonic acids. Fur *et al.* [10] have reported the noncentrosymmetric structures based on 2-amino-5-nitropyridine and chloroacetic acid assemblies. The chemistry of derivatives of barbituric acid is commonly known as barbiturates. The barbiturate is combining with a no. of biological activities such as antibacterial, hypertensive, sedative and as local anesthetic drugs [11-13]. Recent report indicate their applications as antitumor, anticancer and anti AIDS agents [14-16].

Phenylthioacetic acid (PTAA) is a colourless compound, soluble in alcohols. It can be prepared by the subsitution of

sodium chloroacetate with thiophenol or by the analyse of bromoacetic acid with thallium(I) benzothiolate. Derivatives of PTAA (*o*-hydroxyphenylthio)acetic- and benzal-*bis*-(β-thiopropionic) acid show antituberculotic activity [17-19]. Ph-S-CH_2-COOH is used as a free radical quencher in laser flash photolysis experiments [20]. Bacterial infections are commonly conduct with antibiotic chemotherapy. The biological targets of these antibiotics are at the origins of appearance of contrary bacterial strains. Recently, the development of new approaches, such as the 'antivirulence strategy' leads the medicinal chemist to describe novel targets with a reduced probability of resistance development. Virulence factors, such as enzymes involved in the biosynthesis of amino acids, have been approve as such targets [21]. Compounds containing S-aryl ketones are a new class of hesitantly dehydrogenise inhibitors [22].

Phenylthioacetic acid is a fabricated precursor for a variety of Ph-S-containing compounds such as $PhSCH_2$=C=O [23], $PhSCH_2CON$=C=S [23], $PhSCH_2CO_2Me$ [24], $PhSCH_2NO_2$ [25,26], MeCH=C(NO_2)SPh [25,26], $PhSCHClCO_2H$ [27], $PhSCH_2Cl$ [27] and 2-(phenylthio)methyl-1-oxazolidine derivatives [28].

Phenylthioacetic acid has two active sites, the carboxylic acid group and the active methylene group, given that a useful method for construct various cyclic compound [29]. It generates a dianion by the action of equiv of butyl-lithium or lithium iisopropylamide (LDA). Caffeine:β-phenylthiopropionic acid co-crystal was prepared and characterized by Kumaresan *et al.* [30].

EXPERIMENTAL

The FT-IR spectra were record in pellet form with spectral grade KBr on a JASCO FT-IR 410 spectrometer in the area 4000-400 cm^{-1}. The single crystal XRD structures of 2A5NPPTAA and 2A5NPBBA are ascertained using a BRUKER APEX 2 X-ray (three-circle) diffractometer. Amount of data sets were composed at room temperature on a BRUKER SMART APEX 2 X-ray diffractometer.

Synthesis and crystal growth of co-crystal PTAA/BBA with 2A5NP: Equimolar quantities of phenylthioacetic acid (PTAA) and 2-amino-5-nitropyridine (2A5NP) were dissolved in 1:1 v/v aq. methanol. One solution be slowly added into the other with stirring and allow to stand at room temperature. Slow evaporation of the mixture under eminent conditions yield colourless crystals of 2A5NPPTAA in 5 days (Yield: 76 %). Similarly barbituric acid (BBA) and 2-amino-5-nitropyridine (2A5NP) were dissolved individually in 1:1 v/v aqueous methanol. One solution was gradually added into the further with stirring and allowed to stand at room temperature. Slow evaporation solution growth technique of the mixture under ambient conditions yield colourless crystals of 2A5NPBBA in 4 days (Yield: 68 %). The crystallographic data and structure refinement parameters of both crystals are given in Table-1.

X-ray structure: The crystal structures were determined using a BRUKER APEX 2 X-ray (three circles) diffractometer [31]. The absorption correction carried out using the programme SADABS. The structure solution was acquired using SHELXTL (XS) [32] and absence of additional symmetry was proved using PLATON [33]. Olex 2 was utilized for the final data presentation and structure plots [34].

Computational studies: The correct molecular structure and vibrational spectra for 2A5NPPTAA and 2A5NPBB molecules were carried out theoretically by 6-311++ G(d,p) level on an Intel Core i5/3.20 GHz computer using Gaussian 09W [35] program package without any constraint [36]. Initial geometry was taken from the single crystal X-ray studies and it was optimized by Hartee-Fock (HF) method using the 6-311++G (d,p) basis set (Table-2). The molecular geometries be also optimized by density functional theory (DFT) using

TABLE-1
CRYSTALLOGRAPHIC DATA AND STRUCTURE REFINEMENT PARAMETERS

	2A5NPPTAA	2A5NPBB
Empirical formula	$C_{13}H_{13}N_3O_4S$	$C_{14}H_{14}N_8O_7$
Formula weight	307.32	406.33
Temperature	110.15 K	123.15 K
Wavelength	0.71073 Å	0.71073 Å
Crystal system, space group	Triclinic, P-1	Monoclinic, $P2_1/n$
Unit cell dimensions	a =11.805 (2) Å; α = 93.166 (2)°	a = 7.777 (2) Å
	b = 12.188 (5) Å; β = 90.086 (2)°	b = 17.471 (5) Å; β = 95.209 (3)°
	c = 15.094 (3) Å; γ = 107.398 (2)°	c = 12.503 (3) Å
Volume	2068.8 (6) $Å^3$	1691.6 (8) $Å^3$
Z, Calculated density	6, 1.480 Mg/m^3	4, 1.595 Mg/m^3
Absorption coefficient	0.255 mm^{-1}	0.131 mm^{-1}
F(000)	960	840
Crystal size	0.56 × 0.19 × 0.18 mm	0.57 × 0.32 × 0.21 mm
Theta range for data collection	2.00 to 27.47°	2.00 to 27.47°
Limiting indices	$-15 \le h \le 15$, $-15 \le k \le 15$, $0 \le l \le 19$	$-10 \le h \le 10$, $-22 \le k \le 22$, $-14 \le l \le 16$
Reflections collected/unique	14786/14786 [R(int) =]	14547/3841 [R(int) = 0.0368]
Completeness to θ = 25.242	99.9 %	99.8 %
Refinement method	Full-matrix least-squares on F^2	Full-matrix least-squares on F^2
Data/restraints/parameters	14786/0/572	3841/0/262
Goodness-of-fit on F^2	0.988	1.017
Final R indices [I>2σ(I)]	R1 = 0.0614, wR2 = 0.1517	R1 = 0.0395, wR2 = 0.0901
R indices (all data)	R1 = 0.0760, wR2 = 0.1650	R1 = 0.0565, wR2 = 0.0991
Largest diff. peak and hole	0.747 and -0.481 e.$Å^{-3}$	0.235 and -0.265 e.$Å^{-3}$

TABLE-2
IMPORTANT OPTIMIZED MOLECULAR GEOMETRICAL FRAMEWORK FOR skv2

2A5NPPTAA [Bond length (Å)]				2A5NPBB [Bond length (Å)]			
Atom connected	Experimental	HF/6-311++ G(d,p)	B3LYP/6-311++G(d,p)	Atom connected	Experimental	HF/6-311++G(d,p)	B3LYP/6-311++G(d,p)
C5–S1	1.773 (2)	1.789	1.786	C8–O1	1.222 (2)	1.202	1.234
C16–S1	1.809 (2)	1.819	1.824	C9–O2	1.218 (2)	1.185	1.211
C19–O2	1.228 (3)	1.19	1.218	C13-O3	1.212 (2)	1.185	1.211
C19–O3	1.297 (3)	1.31	1.323	C8–N4	1.370(2)	1.363	1.374
C5–C6	1.392 (3)	1.389	1.399	C9–N4	1.365 (2)	1.375	1.388
C5–C14	1.402 (3)	1.389	1.404	C8–N6	1.369 (2)	1.363	1.374
C6–C8	1.386 (3)	1.386	1.396	C13–N6	1.373(2)	1.375	1.388
C8–C10	1.393 (4)	1.385	1.391	C9–C10	1.501 (2)	1.509	1.516
C10–C12	1.388 (4)	1.385	1.396	C10–C13	1.501 (2)	1.509	1.516
C12–C14	1.385 (3)	1.386	1.389	N20–O14	1.235 (2)	1.191	1.229
C16–C19	1.505 (3)	1.507	1.515	N20–O15	1.230 (2)	1.189	1.226
O20–N26	1.232 (3)	1.190	1.228	C21–N16	1.349 (2)	1.33	1.352
O21–N26	1.232 (3)	1.190	1.228	C27–N16	1.331 (2)	1.321	1.333
C27– N22	1.334 (3)	1.337	1.345	C21-N17	1.342 (2)	1.343	1.352
C27–N25	1.357 (3)	1.334	1.357	C26–N20	1.435 (2)	1.445	1.458
C33–N25	1.331 (3)	1.321	1.333	C21–C22	1.411 (2)	1.414	1.418
C32–N26	1.445 (3)	1.443	1.456	C22–C24	1.358 (2)	1.362	1.374
C27–C28	1.416 (3)	1.417	1.421	C24–C26	1.396 (2)	1.397	1.400
C28–C30	1.357 (3)	1.360	1.372	C26–C27	1.372 (2)	1.376	1.389
C30–C32	1.401 (3)	1.399	1.402	O29–N35	1.233 (2)	1.191	1.229
C32–C33	1.375 (3)	1.374	1.387	O30–N35	1.230(2)	1.189	1.226
				C36–N31	1.349 (2)	1.33	1.352
C5–S1–C16	101.9 (1)	99	102.3	C42–N31	1.327 (2)	1.321	1.333
S1–C5–C6	124.4 (2)	120.3	125.5	C36–N32	1.341 (2)	1.343	1.352
S1–C5–C14	116.2 (2)	120.3	115.5	C41–N35	1.447 (2)	1.445	1.458
C6–C5–C14	119.4 (2)	119.5	119	C36–C37	1.411 (2)	1.414	1.418
C5–C6–C8	119.8 (2)	120.2	120.1	C37–C39	1.365 (2)	1.362	1.374
C6–C8–C10	120.9 (2)	120.1	120.8	C39–C41	1.391 (2)	1.397	1.400
C8–C10–C12	119.1 (2)	119.9	119.2	C41–C42	1.374 (2)	1.376	1.389
C10–C12–C14	120.7 (2)	120.1	120.5	C8–N4–C9	126.3 (1)	126.5	126.3
C5–C14–C12	120.1 (2)	120.2	120.5	C8–N6–C13	125.8 (1)	126.5	126.3
S1–C16–C19	110.1 (2)	111.6	110.4	O1–C8–N4	121.4 (1)	121.4	121.3
O2–C19–O3	125.0 (2)	123.7	124.5	O1–C8–N6	121.7 (1)	121.4	121.3
O2–C19–C16	122.9 (2)	124.8	124.1	N4–C8–N6	117.0 (1)	117.1	117.5
O3–C19–C16	112.1 (2)	111.5	111.4	O2–C9–N4	120.8 (1)	121.2	121.1
C27–N25–C33	119.4 (2)	118.9	119.1	O2–C9–C10	122.3 (1)	122.3	122.7
O20–N26–O21	123.6 (2)	124.6	124.6	N4–C9–C10	116.9 (1)	116.4	116.3
O20–N26–C32	118.4 (2)	117.9	117.9	C9–C10–C13	116.7 (1)	116.8	117.5
O21N–26–C32	118.0 (2)	117.5	117.5	O3–C13–N6	120.5 (1)	121.2	121.1
N22–C27–N25	117.0 (2)	117.5	117.1	O3–C13–C10	122.4 (1)	122.3	122.7
N22–C27–C28	122.5 (2)	120.8	121.8	N6–C13–C10	117.1(1)	116.4	116.3
N25–C27–C28	120.4 (2)	121.7	121.1	C21–N16–C27	118.5 (1)	119.1	119.3
C27–C28–C30	119.8 (2)	118.9	119.3	O14–N20–O15	117.4(1)	124.7	124.6
C28–C30–C32	118.5 (2)	118.5	118.5	O14–N20–C26	122.9 (1)	117.4	117.5
N26–C32–C30	120.8 (2)	120.5	120.5	O15–N20–C26	119.6 (1)	117.9	117.9
N26–C32–C33	119.6 (2)	120.3	120.1	N16–C21–N17	121.7 (1)	117.1	116.8
C30–C32–C33	119.6 (2)	119.2	119.4	N16–C21–C22	116.6 (1)	122	121.5
N25–C33–C32	122.3 (2)	122.8	122.5	N17–C21–C22	121.7 (1)	120.9	121.7
				C21–C22–C24	119.3(1)	118.6	119
S1-C5-C6-C8	179.3 (2)	178.8	-179.9	C22–C24–C26	118.1 (2)	118.6	118.6
S1-C5-C14-C12	-179.6 (2)	-178.8	179.9	N20–C26–C24	120.2 (1)	120.3	120.2
S1-C16-C19-O3	-173.2 (2)	-179.9	-179.9	N20–C26–C27	119.6 (1)	120.3	120.2
C5-S1-C16-C19	178.9 (2)	179.9	-179.9	C24–C26–C27	120.2 (1)	119.4	119.6
				N16–C27–C26	122.3(1)	122.4	122.1
				C36–N31–C42	118.9 (1)	119.1	119.3
				O29–N35–O30	117.9 (2)	124.7	124.6
				O29–N35–C41	123.3 (2)	117.4	117.5
				O30–N35–C41	118.8 (1)	117.9	117.9
				N31–C36–N32	121.5 (1)	117.1	116.8
				N31–C36–C37	116.3 (1)	122	121.5
				N32–C36–C37	122.2 (2)	120.9	121.7
				C36–C37–C39	119.0 (2)	118.6	119
				C37–C39–C41	118.3 (2)	118.6	118.6
				N35–N41–C39	121.0 (1)	120.3	120.2
				N35–C41–C42	118.8 (2)	120.3	120.2
				C39–C41–C42	120.2 (1)	119.4	119.6
				N31–C42–C41	122.1 (2)	122.4	122.1

the Becker's three-parameters exchange functional (B3) [37] in combination with the Lee-Yang-Parr correlation functional (LYP) [38]. Then vibration standard nuclear area of the arrangement was used for harmonizing vibration number computation resulting in IR and Raman frequencies. Absolutely, the resolved regular mode oscillation frequency adds thermodynamic equity through the best of analytical mechanism. By between the ends of the Gaussview program [39] with traditional values application, vibration occurrence positions were made with a large amount of accuracy. There is always some ambiguity in important internal coordination. However, the defined coordinate from the complete set match quite well with the motion experiential using the Gaussview program.

RESULTS AND DISCUSSION

Molecular geometry: The asymmetric part of compound 2A5NPPTAA, contains nonprotonated 2-amino-5-nitropyridine and phenylthioacetic acid (PTAA). In 2A5NPBBA, nonprotonated form of two 2-amino-5-nitropyridine (2A5NP) and a barbituric acid (BBA) units exist (Figs. 1 and 2).

The H–N–H bond angle of amine group is 113° for 2A5NPPTAA and 106° for 2A5NPBBA. The results show that the amine group is slightly distorted due to its participation in N–H···O intermolecular hydrogen bond. C–NH_2 [1.333 (2) Å for 2A5NPPTAA and 1.342 (2) Å for 2A5NPBBA] and

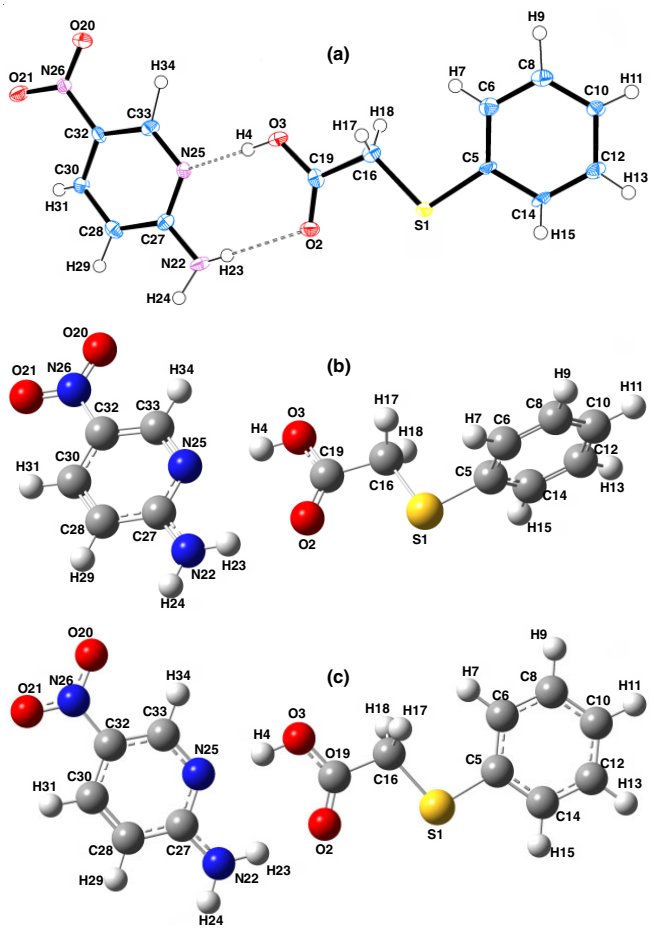

Fig. 1. Molecular structure of the 2A5NPPTAA with the numbering scheme for the atoms and 50 % probability displacement ellipsoids (a) optimized molecular geometry and atomic numbering scheme by HF (b) and B3LYP (c) levels

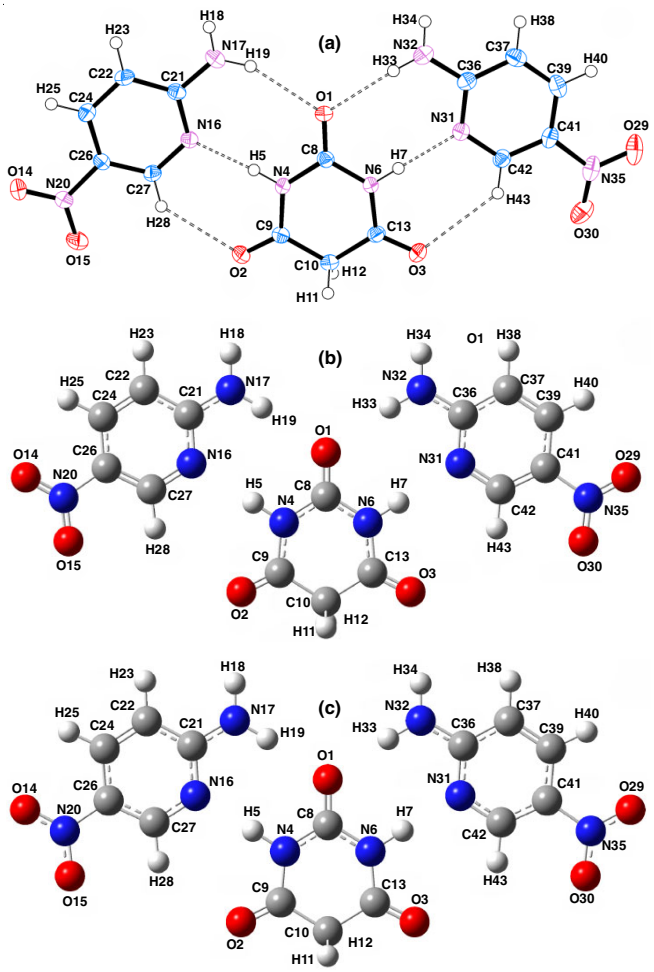

Fig. 2. Molecular structure of the 2A5NPBB with the numbering scheme for the atoms and 50 % probability displacement ellipsoids (a) optimized molecular geometry and atomic numbering scheme by HF (b) and B3LYP (c) levels

C–NO_2 [1.455 (3) Å for 2A5NPPTAA and 1.435 (2) Å for 2A5NPBBA] distances in the 2-amino-5-nitropyridine have been noticed. This bond length is [1.337 (4) and 1.429 (4) Å] slightly deviated from those of the pure 2-amino-5-nitropyridine [40]. The same bond length is observed shortened and lengthened in all the protonated form of 2-amino-5-nitropyridine [41]. In the present case, both bond lengths are found better due to the delocalization of π-bond (Tables 3 and 4).

TABLE-3
HYDROGEN BONDING GEOMETRY OF 2A5NPPTAA

D-H···A (Å, °)	(D-H) (Å)	(H···A) (Å)	(D···A) (Å)	(D–H···A) (°)
N22–H23···O2	0.88	2.04	2.910 (3)	169.6
O3–H4···N25	0.84	1.76	2.586 (2)	168.4

Hydrogen bonding features: The crystal packing of 2A5NPPTAA is stabilized by a combination of N–H···O and O–H···N hydrogen bonds. The pyridine-N atom and amino N atom in 2A5NP are linked with the carboxyl group in PTAA through N–H···O and O–H···N intermolecular hydrogen bonds to form the $R_2^2(8)$ ring motif (Fig. 3). Further, this ring motif are linked with another unit of 2A5NPPTAA through N–H···O inter to make $R_4^4(8)$ motifs. These ring motifs lead to the

TABLE-4
HYDROGEN BONDING GEOMETRY OF 2A5NPBB

D-H···A (Å, °)	(D-H) (Å)	(H···A) (Å)	(D···A) (Å)	(D–H···A) (°)
N6-H7...N31	0.88	1.89	2.769 (2)	175
N6-H5...N15	0.88	1.91	2.787 (2)	173
N4-H34...O2$^{\#1}$	0.95	2.43	3.264 (2)	146
N32-H33...O1	0.94	2.31	3.196 (2)	157
N17-H19...O1	0.88	2.22	3.079 (2)	166
N17-H18...O29$^{\#1}$	0.88	2.14	2.938 (2)	150

Equivalent positions: i. x-1/2,-y+3/2,+z+1/2

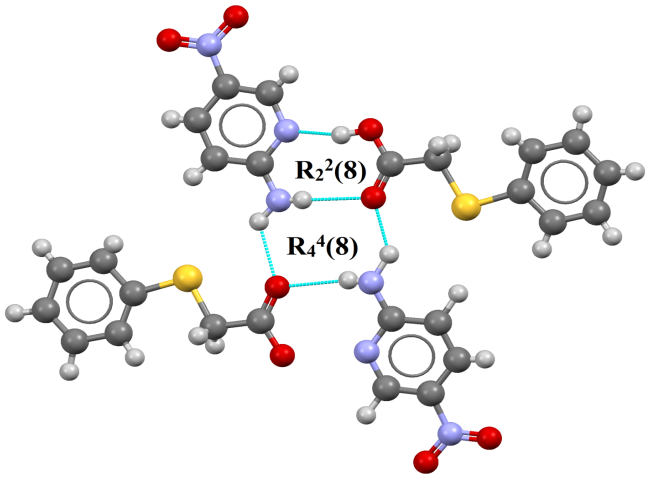

Fig. 3. Molecular aggregation formed through 2A5NPPTAA ring motifs. Hydrogen bonds are shown as dashed lines

hydrophilic layers at z = 0 and 1 which are sandwich between the hydrophobic layer at z = 1/2 (Fig. 4).

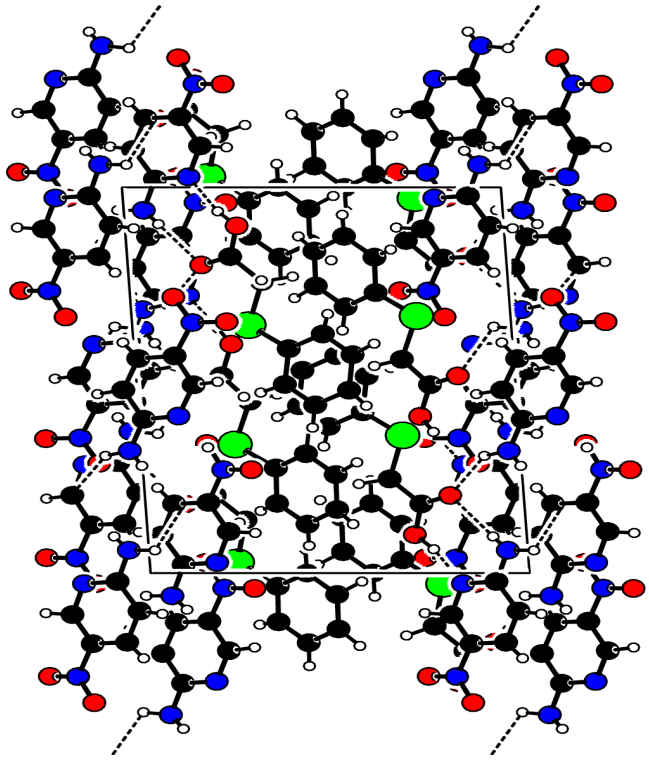

Fig 4. Packing diagram of the 2A5NPPTAA molecules viewed down the a-axis showing alternate hydrophilic and hydrophobic regions at z = 0 or 1 and z = 1/2 respectively. H bonds are drawn as dashed lines

In 2A5NPBBA, the N–H···O and N–H···N intermolecular hydrogen bonds form two $R_2^2(8)$ motifs of a 2A5NP–acid heterosynthon. This ring motif is connected with the nitro group in 2A5NP by N–H···O hydrogen bond to form a rare bifurcated ring $R_3^4(8)$ motif. These two ring motifs are further connected in barbituric (BBA) acid *via*, N–H···O hydrogen bond to form ring $R_3^3(12)$ motifs (Fig. 5). This ring motif is mainly involved by two 2A5NP molecules and a BBA. These ring motifs are aggregated to lead a sheet-like structure along the b-axis (Fig. 6). These molecular aggregations are leading parallel to the 202 and $\bar{2}0\bar{2}$ crystallographic planes making strong force peaks for these planes on X-ray diffraction.

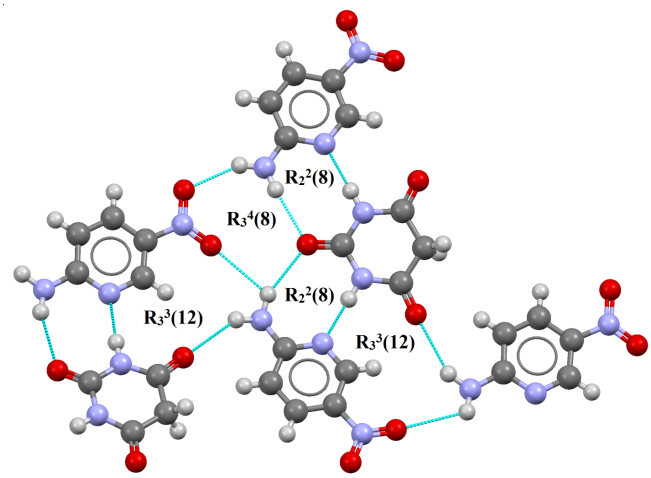

Fig. 5. Molecular aggregation formed through 2A5NPBB ring motifs. Hydrogen bonds are shown as dashed lines

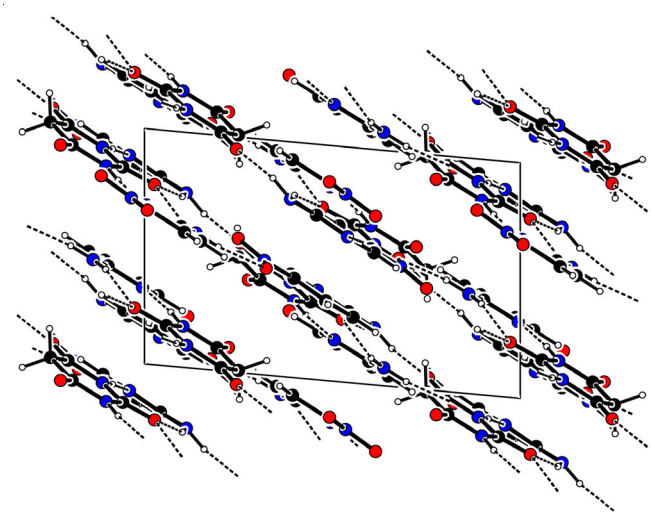

Fig 6. Packing diagram of 2A5NPBB molecules viewed down the b-axis. H bonds are drawn as dashed lines

Mulliken atomic charge analysis: Generally, Mulliken atomic charge result has an important application of quantum chemical calculations to molecular systems. It plays a vital role in the packing of crystals in the solid state by way of intermolecular interaction and it has significant influence on dipole moment, polarizability, electronic structure and vibrational modes [28]. The Mulliken charge analysis of molecules 2A5NPPTAA and 2A5NPBB are calculated at the HF and DFT/B3LYP levels for the molecule under study which

are given in Table-5 and the corresponding population analysis graph are shown in Figs. 7 and 8. The charge circulation of 2A5NP shows that the two carbon atoms attached with hydrogen atoms are negative. All the five carbon atoms in 2A5NP, one of the carbon (C32 for 2A5NPPTAA and C26 and C41 for 2A5NPBB) atoms has more electro negativity than the others; it is due to the carbon atom attached to nitro ($-NO_2$) group. This characteristic nature of carbon atom is to increase the $C-NO_2$ bond distance owing to the electronegative repulsion between these two atoms (carbon and nitrogen). All the hydrogen atoms of 2A5NPPTAA are of positive nature. Moreover, it was identified that the H4 [0.678 *e* for HF and 0.752 *e* for DFT] and H23 [0.459 *e* for HF and 0.391 *e* for DFT] atoms have higher positive charges than the other hydrogen atoms. Because, these two hydrogen atoms are located between or aside the electronegative atoms (nitrogen and oxygen). Further, these two hydrogen atoms are singing vital role in the formation of the intermolecular network in crystalline state. In 2A5NPBB, the hydrogen H5 and H7 [0.677 *e* for HF and 0.691 *e* for DFT] and H19 and H33 [0.475 e for HF and 0.423 *e* for DFT] atoms have higher positive charges than the other hydrogen atoms. This revel the intermolecular charge transmit between the ions and hence the possibility of hydrogen bonding connection and crystal packing. Particularly, the intermolecular charge transfer occurs in the two N-H···O and two N-H···N intermolecular hydrogen bonds.

Vibrational analysis: The vibrational spectroscopy can give important information about the hydrogen bonding forces and strength of intermolecular bonds in addition to regularity of the individual species. The effect of hydrogen bond is very important in crystal environment. The strong, normal and weak hydrogen bonds cause downshifting of stretching mode vibrations and up shifting of deformation mode vibrations with different wave numbers depending upon their strength. Normally, the vibrational shifts of the stretching modes are greater than the bend modes. This indicates that the linear bend is much greater than that of the angular distortion.

The molecular structure of 2A5NPPTAA and 2A5NPBB have various functional groups such as $-NH_2$, $-NO_2$, -NH, -CH, -C–N, -C–C-, -C=O, disubstituted benzene ring, *etc*. The vibrational bands of these groups are predictable to change in their intensity and position due to their environments [42]. Whole vibrational analyses of the 96 fundamental modes of 2A5NPPTAA and 123 original modes of 2A5NPBB are attempted and predicted by the quantum chemical computation and compare with their experimental vibrational spectra. The intended

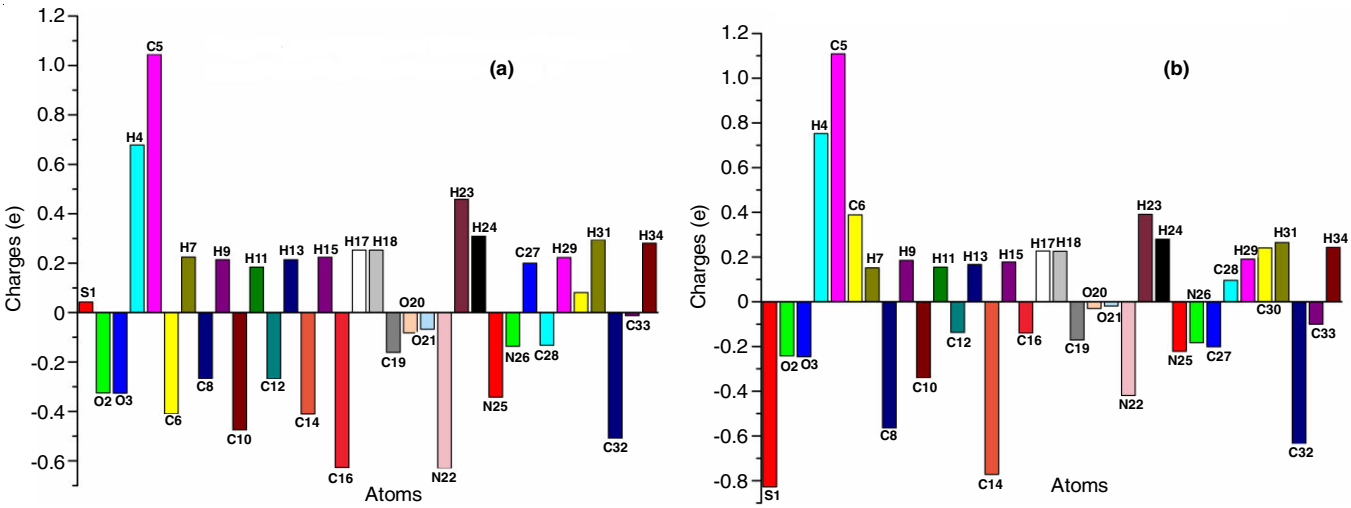

Fig. 7. Atomic charges of the optimized molecular structures for 2A5NPPTAA by (a) HF/6-311++G(d,p) and (b) DFT/6-311++G(d,p) levels

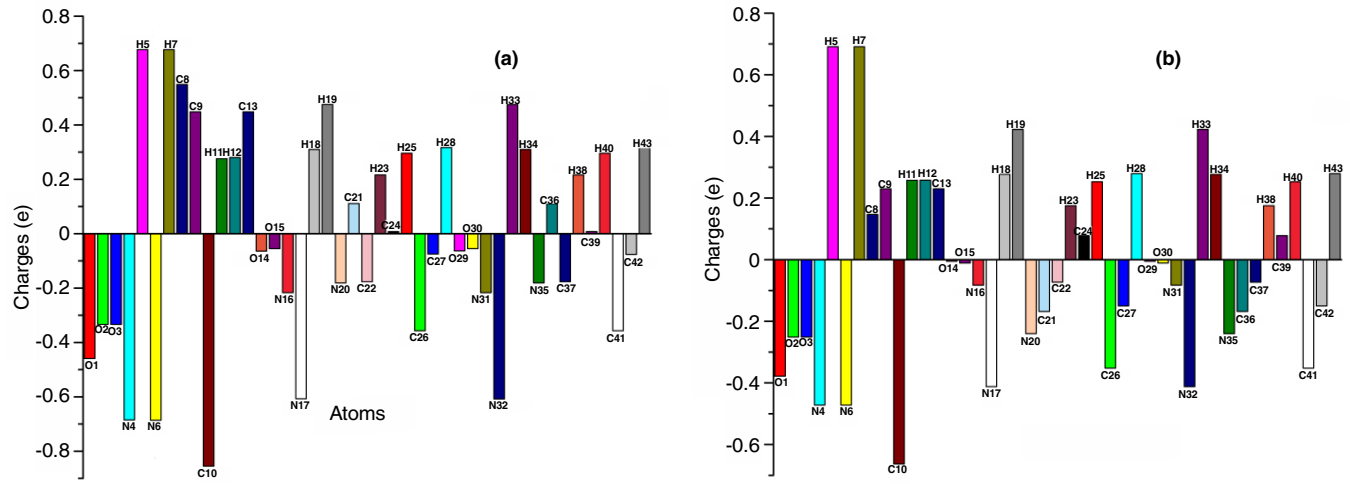

Fig. 8. Atomic charges of the optimized molecular structures for 2A5NPBB by (a) HF/6-311++G(d,p) and (b) DFT/6-311++G(d,p) levels

TABLE-5
MULLIKEN ATOMIC CHARGE
FOR OPTIMIZED CALCULATIONS

2A5NPPTAA			2A5NPBB		
Atom	HF/6-311++G (d,p)	B3LYP/6-311++G (d,p)	Atom	HF/6-311++G (d,p)	B3LYP/6-311++G (d,p)
S1	0.043	-0.828	O1	-0.459	-0.378
O2	-0.325	-0.242	O2	-0.334	-0.251
O3	-0.326	-0.246	O3	-0.334	-0.251
H4	0.678	0.752	N4	-0.685	-0.472
C5	1.045	1.109	H5	0.677	0.691
C6	-0.41	0.389	N6	-0.686	-0.472
H7	0.225	0.152	H7	0.677	0.691
C8	-0.268	-0.564	C8	0.549	0.147
H9	0.214	0.185	C9	0.448	0.23
C10	-0.475	-0.341	C10	-0.855	-0.663
H11	0.184	0.155	H11	0.276	0.258
C12	-0.268	-0.137	H12	0.28	0.258
H13	0.214	0.167	C13	0.448	0.23
C14	-0.41	-0.772	O14	-0.064	-0.005
H15	0.225	0.178	O15	-0.055	-0.011
C16	-0.627	-0.14	N16	-0.217	-0.083
H17	0.253	0.227	N17	-0.607	-0.412
H18	0.253	0.226	H18	0.31	0.277
C19	-0.161	-0.171	H19	0.475	0.423
O20	-0.082	-0.03	N20	-0.181	-0.24
O21	-0.067	-0.019	C21	0.111	-0.168
N22	-0.631	-0.419	C22	-0.177	-0.073
H23	0.459	0.391	H23	0.216	0.175
H24	0.31	0.281	C24	0.008	0.078
N25	-0.342	-0.222	H25	0.296	0.253
N26	-0.136	-0.183	C26	-0.357	-0.352
C27	0.2	-0.201	C27	-0.075	-0.15
C28	-0.132	0.096	H28	0.317	0.279
H29	0.223	0.191	O29	-0.063	-0.005
C30	0.081	0.241	O30	-0.055	-0.011
H31	0.295	0.265	N31	-0.217	-0.083
C32	-0.509	-0.636	N32	-0.608	-0.412
C33	-0.012	-0.1	H33	0.475	0.423
H34	0.281	0.243	H34	0.31	0.277
			N35	-0.181	-0.24
			C36	0.111	-0.168
			C37	-0.177	-0.073
			H38	0.216	0.175
			C39	0.008	0.078
			H40	0.296	0.253
			C41	-0.357	-0.352
			C42	-0.076	-0.15
			H43	0.317	0.279

vibrational wave numbers, measured FT-IR and FT-Raman band positions with their matching assignments for the molecules 2A5NPPTAA and 2A5NPBB are given in Tables 6 and 7, respectively. The FT-IR and FT-Raman spectra of the compounds are shown in Figs. 9 and 10, respectively which are compared with their theoretical counterparts.

Vibrations of the -NH_2: The N–H stretching vibrations from the primary amines occur in the region 3600–3300 cm^{-1} [43,44]. In the present case, the 2-amino-5-nitropyridine has less intense peak calculated at 3941/3694 and 3951/3703 cm^{-1} in HF/B3LYP levels for 2A5NPPTAA and 2A5NPBB, respectively to assign the NH_2 asymmetric stretching modes. This stretching vibration appears as a medium band at 3738 cm^{-1} in

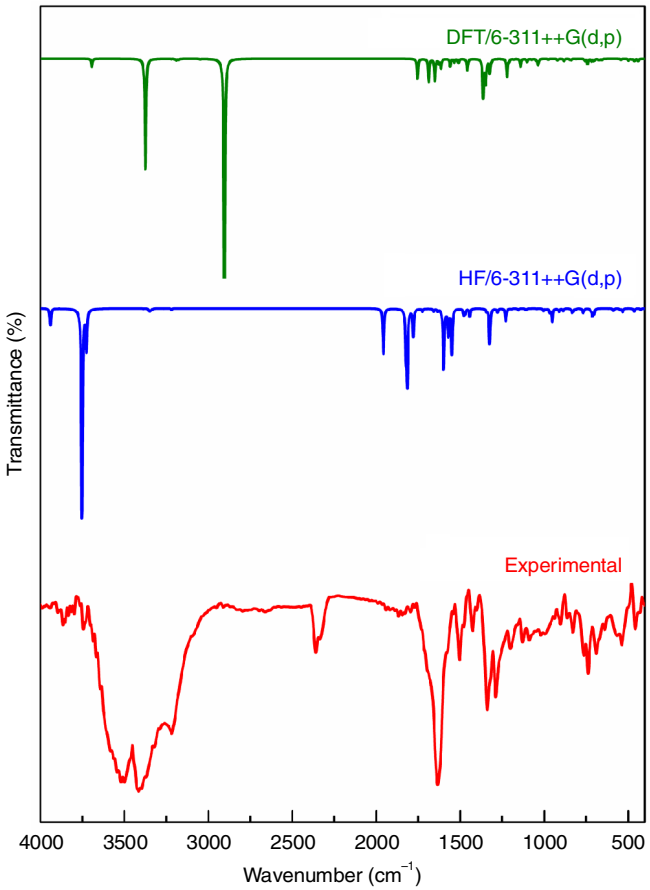

Fig. 9. Comparative representations of FT-IR spectra for 2A5NPPTAA

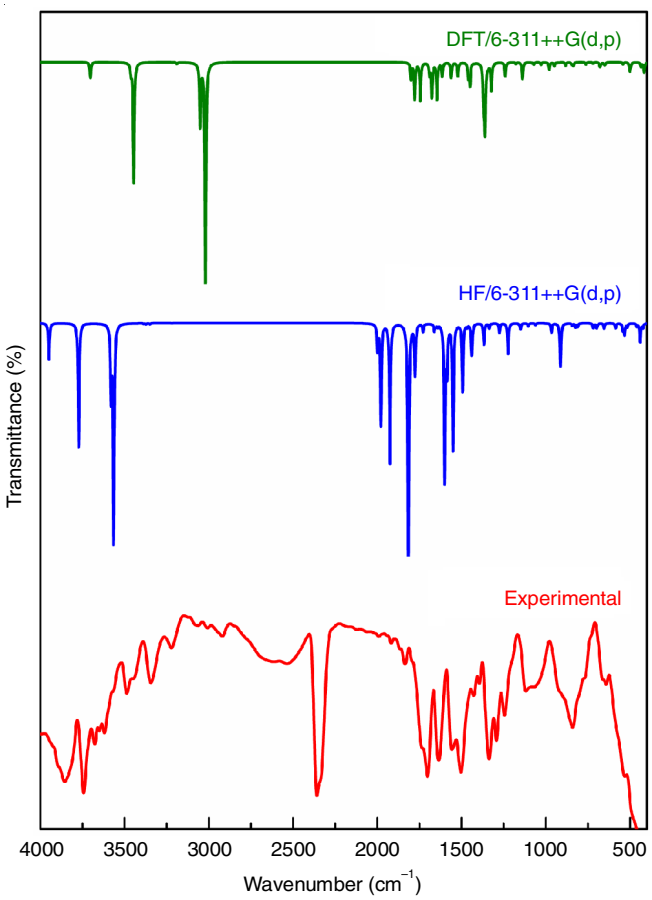

Fig. 10. Comparative representations of FT-IR spectra for 2A5NPBB

TABLE-6
EXPERIMENTAL AND CALCULATED VIBRATION FREQUENCIES (cm^{-1}) OF 2A5NPPTAA

Mode No.	Observational FT-IR	HF/6-311++G(d,p)		B3LYP/6-311++G(d,p)		Position
		ν_{cal}	$*I^{IR}$	ν_{cal}	$*I^{IR}$	
1		13	0.195	13	0.396	γ C–H
2		16	2.647	18	2.227	γ C–H
3		30	2.975	29	0	γ C–H
4		33	0.041	33	2.612	Lattice vibration
5		48	1.392	49	0.005	Lattice vibration
6		59	0.384	51	0.564	ρ CH_2
7		66	2.418	70	4.288	ω CH_2
8		75	5.331	76	6.13	ρ CH_2
9		78	2.517	99	2.141	β C–H
10		99	0.015	104	0.142	ρ CH_2
11		120	3.232	112	1.799	ρ CH_2
12		133	2.405	158	15.149	β C–H
13		225	17.072	183	0.342	γ C–H
14		254	1.855	232	3.919	ρ NO_2 + ω CH_2
15		258	0.329	242	8.585	ρ NO_2
16		286	0.699	264	0	γ C–H
17		311	0.501	295	14.757	β C–H
18		349	159.438	369	0.995	ν C–N + β C–H
19		399	1.149	370	118.129	γ N–O
20		426	9.296	412	0	γ C–H
21		455	0.014	415	0.996	ρ NO_2 + ω CH_2
22		463	0.005	428	0.252	γ C–H
23		464	27.66	440	31.386	ρ NO_2
24		479	0.722	463	31.938	ρ NO_2
25		532	32.255	478	7.921	γ C–H
26		547	12.837	498	27.243	γ C–H
27	528 w	587	20.338	543	15.641	ρ NO_2
28		618	0.61	583	0.036	ρ CH_2
29		673	0.013	631	0.58	Planar ring distortion
30		702	13.371	656	17.444	ν C–C + β C–H
31		703	36.156	668	13.105	ω CH_2 + β O–H
32		713	66.151	676	14.645	ω CH_2
33		722	15.32	700	17.727	γ C–H
34		763	14.117	707	24.899	γ C–C
35		768	36.275	717	33.31	γ (C–H + N–H)
36	728 w	813	7.781	737	7.509	γ C–H
37		826	21.063	742	68.06	γ C–H
38		834	36.533	757	27.563	t NH_2
39		888	22.036	811	2.97	ω CH_2
40		910	30.058	837	0	β C–H
41		920	4.461	839	19.037	β C–H
42		949	9.617	848	10.912	δ NO_2
43		952	117.902	882	33.33	Ring breathing
44		967	35.498	895	0.746	γ C–H
45		989	9.627	915	8.674	ρ CH_2
46		1004	21.495	921	19.397	ω CH_2 + ν C–C
47		1045	3.003	975	13.025	γ C–H
48		1082	1.454	975	0.417	γ C–H
49		1099	1.991	996	0.03	γ C–H
50		1104	0.001	996	0.045	γ C–H
51		1105	9.527	1011	0.251	Planar ring distortion
52		1112	7.419	1031	19.873	β C–H
53		1117	0.029	1036	80.431	γ C–H
54		1118	0.01	1046	19.319	β C–H
55		1153	14.507	1074	13.354	ρ NH_2
56		1162	1.076	1101	38.357	β C–H
57		1194	4.184	1105	9.98	β C–H
58		1198	1.42	1141	109.816	β C–H
59		1228	119.796	1177	0.173	t CH_2
60		1278	34.42	1180	8.79	β C–H
61		1285	1.68	1183	0.4	β C–H
62		1291	2.459	1209	26.31	β C–H

63	1278 w	1313	0.992	1221	248.781	ω CH_2
64		1325	341.505	1313	20.799	ν C–C + β C–H
65		1345	23.033	1324	191.095	β C–H
66	1345 m	1443	74.764	1342	34.62	ω CH_2 + ρ NH_2
67		1444	2.215	1348	311.704	ω CH_2 + β C–H
68		1470	41.319	1358	40.116	β C–H
69		1478	54.913	1363	516.01	β N–H + ρ NH_2
70		1550	429.207	1375	0.981	β C–H
71	1418 w	1571	252.285	1452	23.555	δ CH_2
72		1583	10.034	1457	154.816	δ CH_2
73		1597	242.055	1469	4.213	β C–H
74	1504 w	1600	381.392	1508	20.046	β O–H
75		1633	20.02	1511	37.301	β C–H
76		1658	23.792	1535	48.71	β C–H + δ NH_2
77		1725	27.607	1560	105.371	ν N–O + β C–H
78	1632 s	1754	0.691	1611	2.633	ν C–C + β C–H
79		1770	3.997	1614	125.681	ν C–C + β C–H
80		1780	264.213	1627	60.139	ν C–C
81		1815	675.396	1650	308.22	δ NH_2 + ν C=C
82		1822	371.372	1687	317.518	δ NH_2
83		1957	433.159	1754	279.271	ν C=O
84	2352 w	3219	12.506	2904	3319.705	ν O–H···N
85		3266	1.315	3049	5.882	ν_s CH_2
86		3320	0.269	3094	0.486	ν_{as} CH_2
87		3330	5.004	3161	3.216	ν CH (phenyl)
88		3342	15.41	3168	1.427	ν CH (phenyl)
89		3349	18.725	3178	15.136	ν CH (phenyl)
90		3353	3.623	3187	3.63	ν CH
91		3355	10.183	3191	21.381	ν CH (phenyl)
92		3377	0.948	3199	0.739	ν CH
93		3389	2.322	3203	6.495	ν CH (phenyl)
94	3211 w	3726	383.427	3219	3.587	ν CH
95		3753	2007.893	3375	1531.928	ν_s NH_2
96		3941	161.517	3694	115.149	ν_{as} NH_2

*Calculated infrared intensity.

TABLE-7
EXPERIMENTAL AND CALCULATED VIBRATION FREQUENCIES (cm^{-1}) of 2A5NPBB

Mode No.	Observational FT-IR	HF/6-311++G(d,p)		B3LYP/6-311++G(d,p)		Position
		ν_{cal}	$*I^{IR}$	ν_{cal}	$*I^{IR}$	
1		6	2.62	3	4.212	ρ CH_2
2		13	0.004	15	0	Lattice vibration
3		20	0.002	25	0	Lattice vibration
4		21	1.213	26	1.392	Lattice vibration
5		30	1.357	28	5.894	ρ CH_2
6		34	19.459	33	7.801	ρ CH_2
7		44	4.475	48	0	t NO_2
8		49	0.706	52	6.537	ω CH_2
9		49	0.143	54	1.782	ρ CH_2
10		58	1.558	55	0.893	β C–H + β N–H
11		76	0.003	77	0	γ (C–H+N–H)
12		79	8.635	83	6.6	ρ CH_2
13		87	0.59	97	0.072	γ C–H
14		100	2.472	108	0	ω NH_2
15		111	0.737	109	5.716	ω NH_2
16		117	0.026	114	2.431	β C–H + β N–H
17		119	12.729	131	0.934	β N–H
18		120	0.006	134	0	γ N–H
19		157	9.348	155	1.94	ρ CH_2
20		235	0.03	233	1.433	β C–H + β N–H
21		252	0.221	234	0.011	β C–H + β N–H
22		252	0.738	261	0	γ (N–H + C–H)
23		269	193.514	264	4.149	γ (N–H + C–H)
24		291	0.01	289	0.002	γ N–H
25		296	124.409	315	247.921	γ C–H

26		399	0.639	367	0.123	β C–H + β N–H
27		399	0.191	368	0.466	β C–H + β N–H
28		424	30.891	389	18.774	β C=O
29		441	139.184	416	139.882	β (C=O + N–H)
30		459	13.411	428	0	γ C–H
31		461	8.558	428	0.97	γ C–H
32		462	0.005	434	56.241	ρ NH_2
33		463	0.652	436	7.74	ρ NH_2
34		517	26.839	485	0.768	ρ CH_2
35		533	0.9	496	46.397	ω CH_2
36		534	59.371	500	0	γ C–H
37		534	22.643	501	45.703	γ C–H
38		543	48.906	501	67.464	ω CH_2
39		586	3.462	541	4.948	β C–H + β N–H
40		587	33.471	542	20.324	β C–H + β N–H
41	637 w	647	0.02	631	0	t CH_2
42		655	39.478	644	7.646	Ring breathing
43		692	2.524	650	34.228	ω CH_2 + β N–H
44		695	5.153	656	5.656	ν C–C
45		699	21.609	657	3.728	Ring breathing
46		701	10.914	669	11.407	ν C–N
47		702	3.995	671	0	t NH_2
48		719	21.793	672	0.834	β N–H
49		720	13.574	678	66.289	γ N–H
50		811	0.048	720	0	γ C–H
51		812	25.428	720	15.947	γ (C–H + N–H)
52		824	0.005	749	0	γ C–H
53		824	29.233	749	1.481	γ C–H
54		844	16.898	761	30.266	γ C–H
55		876	0.458	836	0	γ C=O
56		908	0.351	836	50.876	γ C–H
57	845 m	909	0.087	847	21.979	γ C–H
58		914	321.685	847	6.119	β C–H + β N–H
59		920	3.833	882	45.341	Ring breathing
60		920	5.723	883	0.987	Ring breathing
61		968	63.073	921	5.604	ω CH_2
62		968	5.56	934	5.676	β N–H + ω CH_2
63		1000	0.596	943	0	γ N–H
64		1003	0.575	950	55.322	ρ CH_2
65		1062	13.598	979	101.576	γ N–H
66		1104	2.144	992	0	γ C–H
67		1105	17.843	993	0.802	γ C–H
68		1107	4.039	1001	0	γ C–H
69		1107	0.011	1001	1.736	γ C–H
70		1124	0.881	1028	16.189	β C–H
71		1124	0.415	1029	17.387	β C–H
72		1150	23.23	1069	6.495	ρ NH_2
73		1151	22.651	1071	26.136	ρ NH_2
74		1160	4.514	1083	5.992	β N–H
75	1114 w	1225	125.433	1138	160.94	β C–H
76		1225	104.167	1139	77.545	β C–H
77		1276	70.592	1177	18.922	β C–H
78		1276	0.75	1177	2.142	β C–H
79		1320	2.749	1216	0	t CH_2
80		1337	34.433	1240	195.234	ν C–N
81		1337	1.479	1310	9.355	ω CH_2
82		1368	158.289	1323	376.15	β C–H
83		1439	197.018	1324	22.434	β C–H
84	1334 w	1443	74.034	1342	40.883	β C–H + ρ NH_2
85		1443	4.474	1342	6.308	β (N–H + C–H)
86		1468	1.74	1359	0.055	ν C–N + β (N–H + C–H)
87		1468	16.651	1360	934.17	ν C–N + β N–H
88		1495	506.94	1368	480.576	δ CH_2 + β N–H
89		1542	0.396	1370	27.359	β C–H + β N–H
90		1551	889.712	1370	164.083	β C–H + β N–H
91		1554	87.423	1423	6.176	δ CH_2
92		1587	324.196	1450	322.456	β C–H + β N–H

93		1600	905.39	1452	1.187	β C–H + β N–H
94	1493 w	1602	310.954	1460	211.775	ν C–N
95		1643	17.821	1520	96.9	β C–H + β N–H
96		1649	1.912	1522	21.844	β C–H
97		1655	11.948	1523	93.99	β N–H
98		1663	52.068	1558	25.79	β N–H
99		1730	34.727	1562	188.987	ν N–O
100		1730	22.784	1562	16.317	β C–H + β N–H
101		1777	213.386	1615	192.588	ν C–C + β C–H
102		1778	176.433	1617	5.401	ν C–C + β C–H
103	1632 w	1811	124.013	1645	43.665	δ NH_2 + β C–H
104		1817	782.079	1646	485.357	δ NH_2 + β C–H
105		1817	1101.864	1676	492.488	δ NH_2
106		1824	45.308	1690	167.515	δ NH_2
107	1709 w	1926	1036.467	1745	543.507	ν C=O + β N–H
108		1979	760.402	1778	522.387	ν C=O
109	1830 w	2000	190.516	1800	238.954	ν C=O + β N–H
110	2650 br	3220	1.409	3020	3342.73	ν N–H···N
111	2922 w	3268	0.289	3052	901.506	ν N–H···N
112		3352	0.901	3066	0.13	$ν_s$ CH_2
113		3352	7.666	3097	0.881	$ν_{as}$ CH_2
114		3374	4.018	3185	3.191	ν CH
115		3374	5.258	3185	5.279	ν CH
116		3389	2.505	3191	5.998	ν CH
117		3389	2.183	3191	13.059	ν CH
118	3217 w	3566	1620.183	3219	0.969	ν CH
119		3582	526.333	3219	5.802	ν CH
120		3774	919.394	3446	1723.593	$ν_s$ NH_2
121	3478 w	3781	21.787	3462	132.318	$ν_s$ NH_2
122		3949	52.795	3702	16.205	$ν_{as}$ NH_2
123	3738 m	3951	228.749	3703	210.021	$ν_{as}$ NH_2

*Calculated infrared intensity.

IR spectrum for 2A5NPBB. The NH_2 symmetric stretching vibration occurs at 3478 cm^{-1} in IR spectrum for 2A5NPBB. It is not present in 2A5NPPTAA molecule. The above stretching vibration is predicted at 3753/3375 cm^{-1} in HF/B3LYP levels for 2A5NPPTAA and 3781/3462 cm^{-1} in HF/B3LYP levels for 2A5NPBB. The N–H···O hydrogen bond trace is appear as a broad band around 2900–2700 cm^{-1} for 2A5NPPTAA molecule. The corresponding vibrations were calculated at 3219 and 2904 cm^{-1} in HF and B3LYP methods respectively. These calculated stretching vibrations occur as very strong peaks in theoretical methods. In 2A5NPBB, the broad band is appears in the range of 2990–2400 cm^{-1} due to the N–H···N hydrogen bond. The above vibration is predicted as a strong peak at 3220/3020 and 3268/3052 cm^{-1} in HF/B3LYP methods. The occurrence of sharp and broad bands of the spectrum for both molecules in the theoretical and experimental methods is due to the fact that the theoretical computation are carried out in isolated gas state while the crystalline state dominate with the great hydrogen bonding interactions.

The sharp vibration of the amine group appears at 1630–1610 cm^{-1}. In 2A5NPPTAA molecule, the NH_2 scissoring vibration was found to be 1687 and 1650 cm^{-1} in B3LYP method. This scissoring vibration is observed at 1632 cm^{-1} for 2A5NPBB. The corresponding wave number is predicted at 1645 cm^{-1} in B3LYP method. In both molecules, the HF level is more deviated from the DFT level. In lower wave numbers region, most of the bands appears as scissoring, rocking and wag movement vibrations. It is in excellent quality agreement with the investigational results.

C–H, C–N, C–C and C=O vibrations: The C–H stretching vibrations of aromatic compounds are observed in the region 3100–3000 cm^{-1} [45]. In the present case, the C–H stretching vibration appears at 3211 and 3217 cm^{-1} in the IR spectra of 2A5NPPTAA and 2A5NPBB, respectively. The corresponding vibration is well correlated with B3LYP level and slightly deviated from the HF level. The C–H in-plane bending vibration appears as a weak band at 1504 cm^{-1} for 2A5NPPTAA. It is well correlated with the theoretical results. This band is not observed in 2A5NPBB. The C–N stretching vibration is very difficult to be identified, because the mixing of several bands is possible in this wave number region [46,47]. In the present case, the C–N stretching vibration occurs at 1493 cm^{-1} for 2A5NPBB. This vibration is calculated at 1602 and 1460 cm^{-1} in HF and B3LYP methods, respectively. This vibration is not identified in 2A5NPPTAA molecule.

The substitute benzene ring has six C–C stretching vibrations. These vibrations mainly involve 'quadrant stretching' of the phenyl C-C bonds. But there is a little interface with C-H in-plane bending vibration. Two quadrant-stretching components in substituted benzenes are probable to appear in the regions 1620–1585 and 1590–1565 cm^{-1}, respectively. The 1600 cm^{-1} doublet region is not frequency accessible to change the nature of the substitution such as *ortho*, *meta* and *para*. For these types of substitutions, the quadrant stretching vibrations are infrared still because all atoms from the ring are moving to the opposite directions. The C–C stretching vibration mixed with C–H in-plane bending modes is observed in the modes of 78 and 79 for 2A5NPPTAA molecule. This vibration is not

observed in 2A5NPBB molecule. The C=O stretching vibration is observed at 1830 and 1709 cm^{-1} for 2A5NPBB molecule. This vibration is slightly deviate from the calculate results due to the overlapping of N–H in-plane bending vibration. The vibration band is not active in 2A5NPPTAA molecule.

Conclusion

Two co-crystals of 2-amino-5-nitropyridine with phenylthioacetic acid and barbituric acid be grown-up by slow evaporation methods under room temperature. The crystal packing features indicate three dimensional hydrogen bonding network created by the classical N–H···O and N–H···S for 2-amino-5-nitropyridine : phenylthioacetic acid (2A5NPPTAA) and N–H···O and N–H···N for 2-amino-5-nitropyridine:barbituric acid (2A5NPBBA) hydrogen bonds. The N–H···O and N–H···N intermolecular hydrogen bonds are leading to the two $R_2^2(8)$ and $R_4^2(8)$ ring motifs of 2A5NPPTAA. These two ring motifs lead the hydrophilic layers at z = 0 and 1 which are sandwich between the hydrophobic layer at 1/2. The N–H···O and N–H···N intermolecular hydrogen bonds formed a heterosynthon of two $R_2^2(8)$ motifs. It is further linked with the acid through N–H···O hydrogen bond to form ring $R_3^3(12)$ motifs. This molecular accretion are leading parallel to the 202 and $\bar{2}0\bar{2}$ crystallographic planes making strong intensity peaks for these planes at X-ray diffraction. The shifting of vibration bands due to N–H···O and N–H···N intermolecular hydrogen bonds are analyzed. The optimized molecular structure, molecular properties and vibrational frequencies were estimated by quantum chemical calculations with HF and DFT/B3LYP methods invoking 6-311++G(d,p) basis sets. The optimized molecular geometry and calculate vibrational spectra are compared with experimental results which explain significant agreement.

CONFLICT OF INTEREST

The authors declare that there is no conflict of interests regarding the publication of this article.

REFERENCES

1. G.R. Desiraju, *CrystEngComm*, **5**, 466 (2003); https://doi.org/10.1039/b313552g.
2. C.C. Sun and H. Hou, *Cryst. Growth Des.*, **8**, 1575 (2008); https://doi.org/10.1021/cg700843s.
3. A.V. Trask, W.D.S. Motherwell and W. Jones, *Cryst. Growth Des.*, **5**, 1013 (2005); https://doi.org/10.1021/cg0496540.
4. A.N. Sokolov, T.L. Friscic and R. MacGillivray, *J. Am. Chem. Soc.*, **128**, 2806 (2006); https://doi.org/10.1021/ja057939a.
5. M.L. Cheney, G.J. McManus, J.A. Perman, Z. Wang and M.J. Zaworotko, *Cryst. Growth Des.*, **7**, 616 (2007); https://doi.org/10.1021/cg0701729.
6. N.A. Caballero, F.J. Meléndez, A. Niño and C. Muñoz-Caro, *J. Mol. Model.*, **13**, 579 (2007); https://doi.org/10.1007/s00894-007-0184-9.
7. N. Stanley, P.T. Muthiah, S.J. Geib, P. Luger, M. Messerschmidt and M. Weber, *Tetrahedron*, **61**, 7201 (2005); https://doi.org/10.1016/j.tet.2005.05.033.
8. D.E. Lynch and G.D. Jones, *Acta Crystallogr. B*, **60**, 748 (2004); https://doi.org/10.1107/S0108768104023791.
9. H. Koshima, M. Hamada, I. Yagi and K. Uosaki, *Cryst. Growth Des.*, **1**, 467 (2001); https://doi.org/10.1021/cg015542m.
10. Y. Le Fur, M. Bagieu-Beucher, R. Masse, J.-F. Nicoud and J.-P. Lévy, *Chem. Mater.*, **8**, 68 (1996); https://doi.org/10.1021/cm9501731.
11. J.T. Bojarski, J.L. Mokrosz, H.J. Barton and M.H. Paluchowska, in ed.: A.R. Katritzky, Recent Progress in Barbituric Acid Chemistry in Advances in Heterocyclic Chemistry, Academic Press, Inc., New York, vol. 38 (1985).
12. G.L. Patrick, An Introduction to Medicinal Chemistry, Oxford University Press, Oxford, edn 4, pp. 752, (2009).
13. J.T. Bojarski, J.L. Mokrosz, H.J. Bartoñ and M.H. Paluchowska, *Adv. Heterocycl. Chem.*, **38**, 229 (1985); https://doi.org/10.1016/S0065-2725(08)60921-6.
14. K.S. Gulliya, Uses for Barbituric Acid Analogs, US Patent 5869494A (1999).
15. K. Sakai, and Y. Satoh, Barbituric Acid Derivative and Preventive and Therapeutic Agent for Bone and Cartilage Containing the same, International Patent, W09950252A3 (2000).
16. K. Tanaka, X. Chen, T. Kimura and F. Yoneda, *Tetrahedron Lett.*, **28**, 4173 (1987); https://doi.org/10.1016/S0040-4039(00)95570-9.
17. G. Cerbai and G.F. di Paco Boll, *Chim. Farm.*, **103**, 653 (1964).
18. M. Solotorovsky, *Am. Rev. Tuberc.*, **74**, 68 (1956).
19. M. Aydin, N. Arsu, Y. Yagci, S. Jockusch and N.J. Turro, *Macromolecules*, **38**, 4133 (2005); https://doi.org/10.1021/ma047560t.
20. F. Turtaut, S. Ouahrani-Bettache, J.-L. Montero, S. Köhler and J.-Y. Winum, *MedChemComm*, **2**, 995 (2011); https://doi.org/10.1039/c1md00146a.
21. G. Cerbai and G.F. di Paco, *Dissert. Pharm. Pharmacol.*, **20**, 589 (1968).
22. Y. Ohshiro, N. Ando, M. Komatsu and T. Agawa, *Synthesis*, 276 (1985); https://doi.org/10.1055/s-1985-31175.
23. M. Kennedy, M.A. McKervey, A.R. Maguire and S.J. Naughton, *J. Chem. Soc. Perkin Trans. I*, 1041 (1990); https://doi.org/10.1039/P19900001041.
24. M. Miyashita, T. Kumazawa and A. Yoshikoshi, *J. Chem. Soc. Chem. Commun.*, 362 (1978); https://doi.org/10.1039/c39780000362.
25. M. Miyashita, T. Kumazawa and A. Yoshikoshi, *J. Org. Chem.*, **45**, 2945 (1980); https://doi.org/10.1021/jo01303a005.
26. F.G. Bordwell, M.D. Wolfinger and J.B. O'Dwyer, *J. Org. Chem.*, **39**, 2516 (1974); https://doi.org/10.1021/jo00931a011.
27. J.C. Clinet and G. Balavoine, *Tetrahedron Lett.*, **28**, 5509 (1987); https://doi.org/10.1016/S0040-4039(00)96766-2.
28. P. Magnus, M. Giles, R. Bonnert, C.S. Kim, L. McQuire, A. Merritt and N.J. Vicker, *J. Am. Chem. Soc.*, **114**, 4403 (1992); https://doi.org/10.1021/ja00037a058.
29. (a) T. Takahashi, S. Hahiguchi, K. Kasuga and J. Tsuji, *J. Am. Chem. Soc.*, **100**, 7424 (1978); https://doi.org/10.1021/ja00491a056.
(b) M. Wada, T. Shigehisa and K.Y. Akiba, *Tetrahedron Lett.*, **26**, 5191 (1985); https://doi.org/10.1016/S0040-4039(00)98900-7.
30. S. Kumaresan, M. Indrani, R. Ramasubramanian, R. Subha, P.E. Karthik, S. Athavan and F.R. Fronzcek, *Int. J. Curr. Chem.*, **1**, 163 (2010).
31. J.-T. Li, H.-G. Dai, D. Liu and T.-S. Li, *Synth. Commun.*, **36**, 789 (2006); https://doi.org/10.1080/00397910500451324.
32. Bruker APEX2, SAINT and SADABS, Bruker AXS Inc., Madison, Wisconsin, USA (2008).
33. G.M. Sheldrick, *Acta Crystallogr. A*, **64**, 112 (2008); https://doi.org/10.1107/S0108767307043930.
34. A.L. Spek, *Acta Crystallogr. D Biol. Crystallogr.*, **65**, 148 (2009); https://doi.org/10.1107/S090744490804362X.
35. M.J. Frisch, G.W. Trucks, H.B. Schlegel, G.E. Scuseria, M.A. Robb, J.R. Cheeseman, G. Scalmani, V. Barone, B. Mennucci, G.A. Petersson, H. Nakatsuji, M. Caricato, X. Li, H.P. Hratchian, A.F. Izmaylov, J. Bloino, G. Zheng, J.L. Sonnenberg, M. Hada, M. Ehara, K. Toyota, R. Fukuda, J. Hasegawa, M. Ishida, T. Nakajima, Y. Honda, O. Kitao, H. Nakai, T. Vreven, J.A. Montgomery Jr., J.E. Peralta, F. Ogliaro, M. Bearpark, J.J. Heyd, E. Brothers, K.N. Kudin, V.N. Staroverov, R. Kobayashi, J. Normand, K. Raghavachari, A. Rendell, J.C. Burant, S.S. Iyengar, J. Tomasi, M. Cossi, N. Rega, J.M. Millam, M. Klene, J.E. Knox, J.B. Cross, V. Bakken, C.

Adamo, J. Jaramillo, R. Gomperts, R.E. Stratmann, O. Yazyev, A.J. Austin, R. Cammi, C. Pomelli, J.W. Ochterski, R.L. Martin, K. Morokuma, V.G. Zakrzewski, G.A. Voth, P. Salvador, J.J. Dannenberg, S. Dapprich, A.D. Daniels, O. Farkas, J.B. Foresman, J.V. Ortiz, J. Cioslowski and D.J. Fox, Gaussian 09, Revision A.1, Gaussian, Inc., Wallingford CT (2013).
36. H.B. Schlegel, *J. Comput. Chem.*, **3**, 214 (1982); https://doi.org/10.1002/jcc.540030212.
37. P. Hohenberg and W. Kohn, *Phys. Rev. B*, **136**, 864 (1964); https://doi.org/10.1103/PhysRev.136.B864.
38. A.D. Becke, *J. Chem. Phys.*, **98**, 5648 (1993); https://doi.org/10.1063/1.464913.
39. R. Dennington, T. Keith and J. Millam, Gauss View, Version 5. Semichem Inc., Shawnee Mission (2009).
40. F.P. Anderson, J.F. Gallagher, P.T.M. Kenny and A.J. Lough, *Acta Crystallogr. Sect. E Struct. Rep. Online*, **61**, o1350 (2005); https://doi.org/10.1107/S1600536805010433.
41. C.B. Aakeroy, A.M. Beatty, M. Nieuwenhuyzen and M. Zou, *J. Mater. Chem.*, **8**, 1385 (1998); https://doi.org/10.1039/a800073e.
42. I. Sidir, Y.G. Sidir, M. Kumalar and E. Tasal, *J. Mol. Struct.*, **964**, 134 (2010); https://doi.org/10.1016/j.molstruc.2009.11.023.
43. G. Ploug-Sørensen and E.K. Andersen, *Acta Crystallogr. C*, **39**, 112 (1983); https://doi.org/10.1107/S0108270183003790.
44. M. Kurt, M. Yurdakul and S. Yurdakul, *J. Mol. Struct. THEOCHEM*, **711**, 25 (2004); https://doi.org/10.1016/j.theochem.2004.07.034.
45. V. Krishnakumar and R.J. Xavier, *Spectrochim. Acta A Mol. Biomol. Spectrosc.*, **61**, 253 (2005); https://doi.org/10.1016/j.saa.2004.03.038.
46. H. Lampert, W. Mikenda and A. Karpfen, *J. Phys. Chem. A*, **101**, 2254 (1997); https://doi.org/10.1021/jp962933g.
47. C.N. Banwell and E.M. Mccash, Fundamentals of Molecular Spectroscopy, Tata McGraw Hill, New Delhi, edn 4 (1995).